The importance of processing conditions on the biological response to apatites

Cox, Sophie C.; Jamshidi, Parastoo; Williams, Richard; Grover, Liam M.; Mallick, Kajal K.

DOI:
10.1016/j.powtec.2015.06.061

Document Version
Peer reviewed version

Citation for published version (Harvard):
Cox, SC, Jamshidi, P, Williams, R, Grover, LM & Mallick, KK 2015, 'The importance of processing conditions on the biological response to apatites', *Powder Technology*, vol. 284, pp. 195-203.
https://doi.org/10.1016/j.powtec.2015.06.061

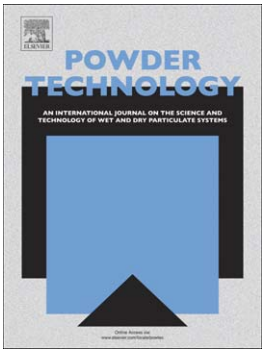

The importance of processing conditions on the biological response to apatites

Sophie C. Cox, Parastoo Jamshidi, Richard L. Williams, Liam M. Grover, Kajal K. Mallick

PII: S0032-5910(15)00520-3
DOI: doi: 10.1016/j.powtec.2015.06.061
Reference: PTEC 11105

To appear in: *Powder Technology*

Received date: 22 May 2015
Revised date: 25 June 2015
Accepted date: 28 June 2015

Please cite this article as: Sophie C. Cox, Parastoo Jamshidi, Richard L. Williams, Liam M. Grover, Kajal K. Mallick, The importance of processing conditions on the biological response to apatites, *Powder Technology* (2015), doi: 10.1016/j.powtec.2015.06.061

The importance of processing conditions on the biological response to apatites

Sophie C. Cox[1], Parastoo Jamshidi[2], Richard L. Williams[1], Liam M. Grover[1*] and Kajal K. Mallick[3^]

[1] School of Chemical Engineering, University of Birmingham, Edgbaston, Birmingham, B15 2TT, UK

[2] School of Metallurgy and Materials, University of Birmingham, Edgbaston, Birmingham, B15 2TT, UK

[3] WMG, University of Warwick, Coventry, CV4 7AL, UK

[*]Corresponding author: tel +44 (0) 121 414 3887, e-mail address l.m.grover@bham.ac.uk

^ Deceased

Abstract

Hydroxyapatite (HA) is commonly synthesised via aqueous precipitation, however, the conditions used are wide ranging. As such, physiochemical properties of HA reported in the literature vary. This work demonstrates that alterations to synthesis conditions have impacts on material chemistry that may be difficult to detect using X-ray diffraction and may compromise substrate cytocompatibility.

Precipitation pH value was shown to be critical to synthesising cytocompatible HA substrates, which support MC3T3 adhesion, spreading, and proliferation. For the first time, pH control during synthesis, at 10 or 11, was demonstrated to improve cellular proliferation; a 49% increase in the number of metabolically active cells at day 7 was observed using an MTT assay. This is explained by the effect of pH on phase purity, stoichiometry, and surface charge. Promisingly, the novel use of a system containing Toluene, a non-polar solvent, reduced crystallinity and increased surface area by 18% compared with apatite produced in deionised water. Ultimately, these physiochemical alterations enhanced the proliferative rate of MC3T3 osteoblast precursor cells by up to 150%.

Keywords: Calcium phosphates; Hydroxyapatite; Aqueous precipitation; Synthesis conditions

1 Introduction

Hydroxyapatite [$Ca_{10}(PO_4)_6(OH)_2$ – (HA)] is an apatitic calcium phosphate (CaP) that has been extensively investigated due to its chemical similarity to the mineral component of hard tissues. Due to the widespread use of this material in bone-related applications (metallic prosthesis coatings, fillers, cements), many methods to synthesise HA have been explored [1-3]. Amongst these techniques aqueous precipitation (AP) is the most common since the reagents involved are of relatively low cost and it is possible to scale the batch size [4].

Despite being widely used, AP reactions are complex due to the simultaneous occurrence of crystal nucleation, growth, coarsening, and agglomeration. The sensitivity of phosphates to synthesis environments and the need to fine tune AP reactions is reflected in the literature by the variability of chemical (e.g. composition) and physical (e.g. particle size and morphology) properties reported for HA when precipitated under different reaction conditions [5-7]. Fundamentally, the solubility of CaPs below pH 8 (except monocalcium phosphate monohydrate), are inversely proportional to pH. Solubility isotherms suggest the pH conditions required for the synthesis of specific CaPs, for example see [8]. HA is the least soluble CaP phase above pH 4.5 and precipitation has been reported between pH levels of 7.5 and 12.5 [9-15]. Under physiological conditions (37°C and pH 7.4) HA exhibits the lowest solubility and thus slowest dissolution rate followed by β-tricalcium phosphate [β-$Ca_3(PO_4)_2$ – (β-TCP)]. Variations of temperature, ionic strength, surfactants and dispersants, as well as maturation time have also been shown to influence the physiochemical properties of precipitated HA [9, 13, 15-19]. Notably, the work of Jarcho *et al.* established the influence of ageing on stoichiometry, as well as other properties, such as strength, of sintered HA [20].

Despite many previous studies being conducted, the role of synthesis and post-treatment parameters is often underestimated [19]. In particular, the effect of changing synthesis

conditions on cellular response is often overlooked [21], despite it being known that physiochemical properties (e.g. crystallinity and surface area), which widely range in the literature, may be key determinants of biological performance [22]. Our previous work has highlighted that pH may affect the cytocompatibility of precipitated HA after 24hrs [23].

The objective of this study is to assess the influence of HA precipitated under varying pH, temperature, and solvent conditions on cell viability over 7 days using a dead/live assay, as well as MTT and Hoechst assays to quantifiably distinguish the degree of MC3T3 cell proliferation. Furthermore, the internalisation of fluorescein stained HA particles by MC3T3 cells was visualised by confocal microscopy.

This study demonstrates that such an approach is crucial in optimising HA. The various synthesis conditions used herein altered both physical and chemical apatite properties, which in turn significantly effected cell viability and proliferation. In particular, observed chemical differences detected by concurrently using simultaneous differential thermal analysis-thermogravimetric analysis (DTA-TGA), Fourier transform infrared spectroscopy (FTIR), and zeta potential (ZP) supported the variation of biological response.

2 Materials and methods

Analytic grade reagents were purchased from Sigma Aldrich (UK) and used without further purification unless otherwise stated.

2.1 Aqueous precipitation of hydroxyapatite

0.05 moles of calcium nitrate tetrahydrate [$Ca(NO_3)_2 \cdot 4H_2O$ >99%] and 0.03 moles of ammonium phosphate dibasic [$(NH_4)_2HPO_4$ >99%] were dissolved separately into 50mL of deionised (DI) water. The pH of these solutions was measured using a pH probe (Tester10,

Eutech Instruments, UK) and then adjusted to the required level using an appropriate amount of aqueous ammonium hydroxide (NH_4OH 28 – 30%). To investigate the influence of Toluene ($C_6H_5CH_3$), 30mL was added to 20mL of DI water to form a 60:40vol% immiscible solution to which 0.05 moles of $Ca(NO_3)_2{\cdot}4H_2O$ was added. For HA synthesised in Ethanolamine (C_2H_7NO), the solvent was added to the Ca^{2+} containing solution under stirring conditions (400rpm) before the adjustment of pH. The solution containing PO_4^{3-} was then added dropwise to the Ca^{2+} solution at room temperature (20°C) while being stirred at 400rpm. Sample coding used in Table 1, for example 10-/RT/DI, indicates the pH level (10) and the degree of pH control during addition (-, i.e. uncontrolled), synthesis temperature (RT – room temperature), and solvent system (DI – deionised water). For samples that were pH controlled (indicated by + in sample coding) during synthesis, this was achieved by adding NH_4OH throughout addition to maintain the reported pH value ±0.1. Once all of the solution containing PO_4^{3-} was added, the suspension was stirred for a further 1.5h at room temperature and the pH was recorded throughout. The formed precipitate was separated from the mother solution by centrifuging four times at 4000rpm for 10mins in a solution of DI water. In between each cycle, the supernatant was removed and fresh DI water added. Finally, the precipitate was washed with DI water, filtered, oven dried at 60°C for 24h, and ground into a fine powder using a pestle and mortar.

2.2 In vitro analysis

2.2.1 Pellet preparation

0.25±0.02g of as-synthesised powders were isostatically pressed into pellets of 10mm diameter by applying a uniaxial force of 800N using a Simplemet 2 press (Buehler, UK). Green pellets were sintered to 600°C at a constant ramp rate of 1°C/min, held at this temperature for 1h and then cooled at a rate of 1°C/min. Cell culture tests were performed by seeding 2×10^4 MC3T3 cells onto the formed pellets.

2.2.2 Live/dead staining

24-multiwell plates were coated with 1.5mL of Sylgard (type 184 silicone elastomer; Dow Corning Corporation, Midland, MI) and left to polymerize for at least a week before use to provide a non-cell-adhesive surface underneath the samples. MC3T3 osteoblast precursor cells were seeded directly onto the surface of HA pellets at a final density of 2×10^4 cells. The viability of the seeded cells was analysed using a Live/Dead® Viability/Cytotoxicity Kit after culturing for 1, 3, 5 and 7 days. Live and nonviable cells were stained with calcein-AM and propidium iodide (1mg/ml; Molecular Probes, Invitrogen), respectively in the dark.

2.2.3 MTT assay

The number of MC3T3 osteoblast precursor cells seeded on the surface of HA pellets was estimated using an MTT assay after culturing for 1, 3, 5, and 7 days. Mitochondria of viable cells reduce the yellow MTT ((3-(4,5-Dimethylthiazol-2-yl)-2,5-diphenyltetrazolium bromide) to formazan, which was dissolved by acidic isopropanol after removal of culture medium. The absorbance of coloured solutions was quantified by measuring at a wavelength of 620nm using a microplate reader (BIO-TEK, US), which gives an indication of cell number at each time point. Tissue culture plastic (TP) surface with identical conditions was used as a control.

2.2.4 Hoechst assay

In order to verify the results of the MTT assay, total DNA was determined using the Hoechst assay. Briefly, each substrate-cell complex was collected at the appropriate time and washed with phosphate buffered saline (PBS). Seeded cells were trypsinized from the surface of the samples and then the cell pellets stored at -80ºC until the end of the experimental period (7 days). All detached cells from different days were thawed to room temperature and 100µL distilled water was added per sample. The solution was incubated at 37ºC for 1h and then they were stored at -80ºC for 20mins and thawed to room temperature again. 100µL of

aqueous Hoechst 33258 in TNE buffer solution was added to each sample. Fluorescence measurements were carried out using a microplate reader (BIO-TEK, US) with excitation at 360nm and detection at 460nm.

2.2.5 Fluorescence staining to visualise cellular internalisation of HA particles

A stock solution of 5mg Fluorescein-5-Maleimide (Life Technologies, UK) in 1mL of PBS was prepared. 1mg of HA particles was suspended in 500µL of PBS and sonicated for 5mins before adding 400µL of Fluorescein stock solution. The HA-Fluorescein mixture was left to react on a thermoblock mixer at 37°C and 1400rpm for 2h. The stained particles were finally washed five times with PBS.

MC3T3 osteoblast precursor cells were seeded at a density of $3x10^4$ cells per quadrant in a 4-segmented live cell imaging dish (Greiner-Bio One Ltd, UK) and incubated overnight at 37°C in supplemented DMEM media. 1mg of HA-dye stock was resuspended in 1mL of supplemented DMEM and diluted into aliquots of 2.4µg/mL. 500µL of supplemented DMEM and 500µL of the diluted HA-dye solution was added to each quadrant of the imaging dish thus giving a final particle concentration of 1.2µg/mL. Imaging was performed after 24h.

2.2.5 ANOVA test

A one-way analysis of variance (ANOVA) test was performed to ascertain whether cell proliferation occurred within the MTT and Hoechst assays. Calculated F ratios were compared with critical F values (F_{crit}) to determine any statistical significance. The level of statistical significance was set at $p<0.05$ and thus the critical values for MTT and Hoechst assay are 4.965 [$F_{crit}(1, 10)$] and 7.709 [$F_{crit}(1, 4)$], respectively.

2.4 Material characterisation

To confirm the crystalline phase composition of samples, XRD was performed on as-synthesised and calcined powders heated to 600°C (sintering temperature of pellets used for cell culture) using a ramp up/down rate of 1°C/min and a hold time of 1h. Furthermore, samples 10-/RT/DI, 11-/RT/DI, 10+/RT/DI, 11+/RT/DI were heated to 900°C to assess stoichiometry of the as-synthesised phase. XRD data was collected on a D5000 diffractometer (Bruker, UK) in Bragg-Brentano geometry over the range $2\theta = 25 – 36°$ using a step size of 0.02° and a count time of 15s. Patterns were matched to JCPDS standards. Line broadening analysis was performed on the (002) peak of as-synthesised HA samples to assess crystallite size (Equation 1).

$$L = \frac{K\lambda}{B\cos\theta} \qquad \text{(Equation 1)}$$

where L = crystallite size, K = Scherrer constant (≈0.9), λ = X-ray wavelength (CuK_{α}=1.54056Å), B = peak width (in radians), and θ = Bragg angle. The (002) diffraction peak was specifically chosen since it is isolated from other characteristic HA peaks.

Spectra of finely ground as-synthesised powders were recorded in ATR mode using a Spectrum One FTIR Spectrometer (Perkin Elmer, UK). IR spectra were collect between 550 and 4000cm^{-1} with a 4cm^{-1} resolution averaged over 8 scans using Spectrum software.

The thermal behaviour of dried powders was determined by simultaneous DTA-TGA using a TGA/DSC-1 STARe instrument (Mettler-Toledo, UK) with STARe software. 10±5mg of samples were heated in alumina crucibles from 30 – 1300°C at a constant ramp rate of 20°C/min in flowing air. A reference alumina crucible was used and data collected for an empty crucible under the same conditions was blank-subtracted.

The morphology and size of as-synthesised particles as well as the surface of prepared pellets were analysed using a Supra55 FEGSEM scanning electron microscope (Zeiss, UK)

operating at 20kV. Prior to analysis, powders and pellets were sputter-coated with a thin layer of gold in an argon-purged chamber for 90s.

An ASAP 2020 surface area analyser (Micromeritics, US) was used to determine the surface area of dried powders. Samples were prepared by heating to 30°C at 1°C/min, evacuated until the pressure reached 10μmm Hg and maintained under these conditions for 10mins. BET analysis was carried out on data between relative pressures of 0.06 and 0.2.

A Zetasizer ZS (Malvern, UK) was used to determine the zeta potential (ZP) of the precipitates in DI water. Dilute suspensions of particles were prepared at 0.1wt% and loaded into zeta cells. Prior to measurement, the cell was agitated in an ultrasonic bath and equilibrated at 25°C for 2mins. Three measurements were taken to obtain an average value.

A fluorescence microscope fitted with a mercury lamp (Carl Zeiss Ltd, UK) was used to visualise live (green) and dead (red) cell cultures on the surface of pellets at magnifications of x20. Fluorescein stained samples were imaged with a Zeiss LSM 710 ConfoCor3 confocal system (Carl Zeiss Ltd, U.K.) attached to a Zeiss Axio Observer.Z1 inverted microscope and equipped with a Zeiss EC Plan-Neofluar x63 NA = 1.40 oil objective lens, 488nm laser diode, 458nm/488nm beam splitter and a 34-channel spectral detector, which was used to divert fluorescence between 500nm and 650nm to a photomultiplier tube detector. Bright field images were obtained simultaneously with the fluorescence images by detecting the transmitted excitation laser light with a second photomultiplier detector [24].

3 Results

3.1 Crystal structure

Formation of HA in all samples was indicated by the characteristic peak occurring at 2θ = 31.77° and verified by matching to the JCPDS pattern for HA (09-432). Notably, sample 10-

/RT/DI exhibited a higher intensity between 2θ = 28 – 30°, which suggested the presence of a trace amount of brushite ($CaHPO_4 \cdot 2H_2O$ - DCPD) (09-0077). Figure 1 demonstrates the relative sharpness of (211), (112), and (300) HA peaks observed in sample 10-/RT/DI (black line) compared to those prepared under controlled pH 11 conditions (i.e. 11+/RT/DI – red line). Furthermore, characteristic peaks of samples synthesised in systems containing Toluene (11+/RT/T and 11+/RT/ET) were shown to be significantly broader compared to precipitates prepared in other solvents (Figure 1 – green and purple lines, respectively). Crystallites sizes of all as-synthesised samples showed no significant variation; all were calculated to be between 20 and 24nm (Table 2).

Secondary phases were not identified in any samples heated to 600°C and no discernible increase in the intensity of characteristic peaks was observed. When specimens 10-/RT/DI, 11-/RT/DI, 10+/RT/DI, 11+/RT/DI were heated to 900°C XRD analysis revealed the presence of β-TCP (JCPDS 09-0169) in all four samples, and β-calcium pyrophosphate (β-$Ca_2P_2O_7$ – JCPDS 09-0346) in 10-/RT/DI (Figure 2). This indicates that as-synthesised samples were non-stoichiometric HA, i.e. calcium deficient HA (CDHA). Noticeably, the intensity of β-TCP diffraction peaks were substantial lower in 10-/RT/DI compared with samples prepared under all other pH conditions, suggesting this as-synthesised phase was closer to stoichiometry.

3.2 IR spectroscopic analysis

Generally, strong characteristic bands at approximately 566, 574, 600, 961, 1030 and 1090cm^{-1} corresponding to PO_4^{3-} vibrations were detected in all samples. Figure 3 illustrates spectra for samples 10-/RT/DI, 11-/RT/DI, 10+/RT/DI, 11+/RT/DI, and 11+/RT/T, which each exhibited different intensities for characteristic PO_4^{3-} vibrations. The spectrum for sample 11+/RT/DI was representative of all other samples not shown in Figure 3. Weak structural OH^- bands detected between 632 and 635cm^{-1} and absorbed H_2O vibrations located

2500 – 3750cm^{-1} exhibited negligible intensity relative to PO_4^{3-} assignments, which may be associated with the relatively short ageing time used (1.5h). Data collected 1750 – 4000cm^{-1} and 550 – 1750cm^{-1} were plotted on different scale y_{left} and y_{right} axes, respectively in Figure 3 to enable better visualisation of absorbed H_2O banding. A band at 875cm^{-1}, associated with HPO_4^{2-}, was assigned in spectra of all samples, which corroborates that the samples were non-stoichiometric CDHA as seen with XRD analysis of sintered precipitates (Figure 2). Interestingly, a weak band that may be associated with a PO stretch in acidic phosphate phases was detected in sample 10-/RT/DI between 1250 and 1550cm^{-1} (Figure 3 – black line).

3.3 Thermal behaviour

TGA data collected between 30 and 1300°C was differentiated (DTG) to enable temperature regions, where a change in the rate of weight loss occurred, to be distinguished. An endothermic peak was demonstrated for all samples below 200°C and this weight loss was attributed to the removal of non-bound surface water. Notably, samples prepared at pH 10 (10-/RT/DI and 10+/RT/DI) exhibited a DTG peak between 200 and 300°C that was associated with a corresponding endotherm (Figures 4a and 4b). A relatively gradual loss of weight 250 - 700°C was demonstrated for all samples. Between 700 and 800°C in all samples except 10-/RT/DI (Figure 4a), and 11+/70/DI (Figure 4d) a rapid endothermic loss of weight was exhibited. All different combinations of DTG peak profiles are shown in Figure 4. Profiles for samples 11-/RT/DI, 11+/RT/E, 11+/RT/T, and 11+/RT/ET are not shown in Figure 4 but exhibited the same combination of DTG peaks as sample 11+/RT/DI (Figure 4c) and comparable total weight losses; 8.3 – 9.3wt% compared with 8.3wt%.

3.4 Zeta potential

The ZP of samples was measured in DI water at 25°C (Table 2). Interestingly, samples 10-/RT/DI and 11+/70/DI exhibited positive ZP values compared to all other samples, which exhibited a negative charge. For those samples with a negative charge and prepared under different pH conditions, an increase in the ZP value was observed with increasing pH or control, i.e. (|11+/RT/DI|>|10+/RT/DI|>|11-/RT/DI|). The solvent system was also shown to significantly influence ZP value, which is to be expected since DI water is polar compared to Ethanolamine and Toluene, which are both non-polar solvents.

3.5 Surface area

Precipitation at pH 10 without control (10-/RT/DI) was found to significantly reduce (>27%) particle surface area compared with all other synthesis conditions (Table 2). Notably, an increased synthesis temperature (11+/70/DI) and precipitation in a Toluene and DI water system (11+/RT/T) were shown to increase surface area by 24 and 18%, respectively compared with sample 11+/RT/DI.

3.6 Particle morphology

Typical micrographs of particles (not shown) revealed globular morphologies and bulk agglomeration in all samples. Agglomerates were approximately sized between 10 and 50μm and exhibited no significant change in morphology from our previous work [23].

3.7 Live/dead staining

Seeding of cells on samples 10-/RT/DI and 11+/70/DI resulted in the death of the cell population (red) at day 1 (Figure 5a) and day 3 (Figure 5c), respectively, indicating a cytotoxic effect of these materials on MC3T3 cells. These samples were therefore not included in the remainder of the *in-vitro* studies. Fluorescence micrographs of all other

samples demonstrated the viability (green) of MC3T3 osteoblast precursor cells from days 1 – 7 of culture (Figure 6 – 11+/RT/DI). The extent of dead cells (red) observed were minimal and therefore associated with the sensitivity of cells to the procedure followed. Live cell density on these samples was clearly shown to increase and the typical morphology changed from rounded (day 1 – Figure 6a) to elongated (day 7 – Figure 6d) over the culture period. These results advocate that these prepared substrates were cytocompatible and supported the adhesion, spreading, and proliferation of MC3T3 osteoblast precursor cells.

3.8 MTT assay

An increase in the metabolic activity of MC3T3 cells seeded on apatite substrates and tissue culture plastic (TP) was observed over the culture period (Figure 7). Proliferative rates were calculated by comparing absorbance values at day 1 with day 7 and the increase in metabolic activity for all substrates was confirmed to be statistically significant ($p<0.05$) using a one-way ANOVA test (Table 3). These results suggest that the control of pH (10+/RT/DI and 11+/RT/DI) compared with adjustment (11-/RT/DI) improved the ability of the substrate to support MC3T3 proliferation. The metabolic activity of cells seeded on apatite substrates prepared in Toluene and DI water solvent system (11+/RT/T) at days 5 and 7 was notably higher compared with other substrates and this accelerated proliferation is highlighted by the significantly larger degree of proliferation, 193.5%, which was more than double the rate of all other solvent systems. In particular, this sample exhibited a relatively high particle surface area and low zeta potential value (Table 2).

3.9 *Hoechst assay*

An increase in the average fluorescence measured on the basis of DNA content using a Hoechst 33258 dye was observed for MC3T3 cells seeded on all samples over the culture period, which corresponds to an increase in cell number (Table 3). ANOVA testing

confirmed that the increase in cell number at day 7 compared with day 1 was significant for all samples except 11-/RT/DI, which supports the assertion that pH control may positively impact cell proliferation. These results support the trends observed for the MTT assay within experimental errors.

3.10 Cellular internalisation of HA particles

In order to determine if the impurity phase (detected by XRD and FTIR) or positive ZP was the source of cytotoxicity demonstrated for sample 10-/RT/DI, combined bright field and confocal fluorescence images of MC3T3 cells exposed to powders prepared under different pH conditions were collected. These images revealed cellular internalisation and cell membrane association for samples that exhibited positive [10-/RT/DI (Figure 8a-c)], and negative [11-/RT/DI (Figure 8d-f), 10+/RT/DI (Figure 8g-i) and 11+/RT/DI (Figure 8 j-l)] ZPs. Therefore suggesting the presence of an acidic impurity phase in sample 10-/RT/DI was the reason MC3T3 cells became non-viable when seeded on this sample after 24hrs.

4 Discussion

XRD patterns of as-synthesised and samples heated to 600°C were matched to HA and no secondary phases were identified (Figure 1). Corresponding FTIR spectra revealed the presence of HPO_4^{2-} (Figure 3), which suggests that precipitates were CDHA. A number of authors have shown that the Ca:P ratio of HA develops towards stoichiometry during maturation [19, 25], and thus the relatively short ageing time (1.5h) may explain why the Ca:P is expected to be <1.67. Furthermore, a short maturation time is suggested to explain the relatively high degree of characteristic XRD peak broadening demonstrated in all precipitated samples, which is synonymous with a low crystalline fraction [19]. In particular, samples prepared in a solvent system containing Toluene (11+/RT/ET and 11+/RT/T) exhibited

broader characteristic peaks compared with 11+/RT/DI, which suggests this non-polar solvent influences the crystallisation process of HA (Figure 1). This is explained in terms of a reduction in the dielectric constant of the solvent system causing an increase in the rate of precipitation of polar molecules since the relative supersaturation level is lower. It is suggested that the use of Toluene increased the rate of HA precipitation; i.e. more and smaller crystals were formed, resulting in broader XRD peaks. Concurrently, faster stabilisation of HA in a less polar system may explain the larger surface areas exhibited by 11+/RT/ET and 11+/RT/T compared with 11+/RT/DI (Table 2). Notably, when compared with stoichiometric HA (=100) bone apatite exhibits a crystallinity of 33 – 37 and numerous studies in the literature support the assertion that there is an inverse relationship between crystallinity and osteoblast differentiation [26, 27].

Concurrent characterisation of samples by XRD and DTA-TGA revealed a number of high temperature phase changes that were associated with endothermic weight loss regions (Figures 2 and 4). Interestingly, for samples 10-/RT/DI and 10+/RT/DI a DTG peak was observed between 200 and 300°C (Figure 4). In addition, FTIR revealed the presence of an acid phosphate phase in 10-/RT/DI (Figure 3) and therefore weight loss within this temperature may be associated with the dehydration of DCPD to monetite ($CaHPO_4$ - DCPA), which is reported to occur at approximately 180°C [28]. It is probable that this secondary phase formed during synthesis since the pH value was not controlled during addition and reached a final value of 5.60 before the precipitate was removed from the mother solution. As the solution pH decreased from 10, particularly below 9, the balance of phosphate ion species begins to shift away from PO_4^{3-} and towards protonated HPO_4^{2-} species. Protonation of PO_4^{3-} as a result of decreasing pH follows the pattern: PO_4^{3-}, HPO_4^{2-}, $H_2PO_4^{2-}$, to H_3PO_4. In contrast, no secondary phases were detected in 10+/RT/DI. When comparing the thermal behaviour of 10-/RT/DI and 10+/RT/DI, the major variance is the

absence of a rapid weight loss region 700 - 800°C for 10-/RT/DI (Figure 4). The gradual weight loss recorded for all samples 250 - 700°C is attributed to the dehydration of HPO_4^{2-}, which was detected in FTIR spectra (Figure 3), to β-$Ca_2P_2O_7$ that has previously been reported to occur within this temperature range [29]. Any formation of $P_2O_7^{4-}$ may subsequently lead to a reaction with OH^- between 700 - 800°C that forms HA and β-TCP [29]. Therefore DTA-TGA results further suggest that all samples were non-stoichiometric HA (i.e. CDHA) and this explains the formation of β-TCP in XRD patterns of samples heated to 900°C (Figure 2). Likewise, the work by Jarcho *et al*. [20], who used a similar synthesis procedure, revealed the presence of large amounts of β-TCP in sintered (1100°C) HA when precipitates were aged for less than 2hrs, which was attributed to non-stoichiometry of the initial phase. The presence of β-$Ca_2P_2O_7$ peaks in the pattern of 10-/RT/DI heated to 900°C and the absence of a DTG peak between 700 and 800°C suggest this sample contains less HPO_4, which may be due to the presence of other acid phosphate phases. Elliot reported that CDHA prepared via the hydrolysis of DCPA would demonstrate weight loss between 250 - 300°C, which is suggested to explain the DTG peak exhibited for 10+/RT/DI within this temperature range [30]. The authors recognise that it is unlikely that DCPA would form under the bulk pH conditions (9.83 - 10.09) recorded during the precipitation of 10+/RT/DI, however, there are many reports in the literature that advocate that an unstable precursor phase can form prior to HA [31-34]. Due to the vast number of ionic species within the precipitation solution is it also plausible that local variation in pH occurred and thus the authors suggest is it probable that 10+/RT/DI formed via an unstable transitional phase.

It is well known that surface charge plays a key role in the adhesion process of cells and the morphology of adhering cells has been shown to depend on the sign of any charge [35]. The ZP of as-synthesised apatites were negative apart from samples 10-/RT/DI and 11+/70/DI (Table 2), which interestingly were both shown to elicit a cytotoxic cellular response (Figure

5). It is suggested that the positive ZP exhibited by 10-/RT/DI is due to the presence of trace amounts of an acidic phosphate phase formed under the pH values reached during synthesis. No secondary phases, however, were identified in sample 11+/70/DI by either XRD or FTIR. The change in surface chemistry, demonstrated by the increase in ZP value from 11+/RT/DI → 10+/RT/DI → 11-/RT/DI, can be linked to the increasing control of a basic precipitation environment. At a higher pH value or under controlled conditions the relative concentration of OH^- is maintained throughout crystallisation and as a result the degree of surface charge is increased. It is likely that the negative surface charge exhibited is created by deprotonation of HA in the OH^- rich environment. The ability of non-polar solvents to influence surface charge is significantly less and this explains why partial replacement of DI water with Toluene (11+/RT/T) resulted in a lower degree of electrostatic stabilisation, i.e. a lower ZP value, compared with 11+/RT/DI. In terms of Ethanolamine, its use resulted in a lower amount of NH_4OH being required to control pH during precipitation and hence the solvent system exhibited a relatively low OH^- intensity. This is suggested to explain the lower ZP value of 11+/RT/E compared with 11+/RT/DI. The lowest degree of electrostatic stabilisation was exhibited by 11+/RT/ET, as may be expected, due to the combined effects of Toluene and Ethanolamine.

Fluorescence micrographs of all samples, except 10-/RT/DI and 11+/70/DI, demonstrated the ability of substrates to support the adhesion, spreading and proliferation of osteoblast precursor cells as evidenced by an increase in cell density and a change in morphology from rounded to elongated over the culture period (Figure 6). These results advocate that the use of Toluene and/or Ethanolamine in the synthesis solvent system did not affect the cytocompatibility of apatites.

Interestingly, lower proliferative rates were revealed for cells seeded on 11-/RT/DI compared with 10+/RT/DI and 11+/RT/DI calculated from MTT and Hoechst data (Table 3).

Furthermore, ANOVA testing demonstrated that the increase in cell number for 11-/RT/DI recorded for the Hoechst assay was not statistically significant. No obvious difference in bulk composition between these samples was demonstrated by XRD or FTIR. Thus, attention was focused on the development of pH during precipitation. Since the pH value was uncontrolled during the precipitation of 11-/RT/DI it is likely that greater shifts in the balance of different ionic species occurred, which may have resulted in a change in surface chemistry compared to samples produced under controlled pH conditions (10+/RT/DI and 11+/RT/DI). This explanation is supported by ZP measurements, which demonstrate variation in value between these samples (Table 2).

In comparison to apatite prepared in DI water (11+/RT/DI), the increase in metabolically active cells between days 1 and 7 was 58 and 15% less for 11+/RT/E and 11+/RT/ET, respectively. In contrast, the proliferative rate of MC3T3 cells seeded onto 11+/RT/T was more than double 11+/RT/DI, this effect may be considered promising since it may translate to improved osteogenesis. Notably, 11+/RT/T exhibited a relatively large surface area and high degree of XRD peak broadening, therefore it may be considered sensible to assume that either or both of these physiochemical properties contributed to the observed increase of cellular metabolic activity. Numerous authors support the assertion that there is an inverse relationship between crystallinity and mineralisation, gene expression of osteonectin as well as osteopontin, and alkaline phosphatase [36-40]. These observations were explained in terms of the improved degradation of less crystalline HA and the ability of these surfaces to provide a dynamic zone for dissolution and re-precipitation [27]. A larger surface area has also been reported as advantageous for osteointegration and osteoconduction [41, 42]. Hence it is concluded to be promising that the use of Toluene was shown to reduce crystallinity and concurrently increase particle surface area of HA precipitates. In contrast, the proliferative rates calculated from DNA straining using a Hoechst dye demonstrated the greatest increase

in cell number for 11+/RT/ET compared with other solvent systems. The degree of proliferation measured from MTT and Hoechst assays performed in this study present a dissimilar assessment of cell proliferation, which may be expected since these values were obtained by measuring different cellular properties. Generally the results obtained from both of these assays, however, advocate that HA substrates prepared in solvent systems containing Ethanolamine and/or Toluene in combination with DI water supported cell proliferation to a higher degree than when seeded on HA prepared under the same reaction conditions in DI water. Overall, variation of the dielectric constant of the solvent system used for precipitation of HA was shown to influence a number of physiochemical properties, in particular the degree of crystallinity, surface area, and ZP. In turn, it was shown that these characteristics may translate to differences in the ability of cells to adhere and proliferate on prepared substrates. It is also important to note that the altered biological responses observed for apatite samples prepared under different conditions may have been influenced by changes in the ionic composition of the DMEM during the experiment since CDHA has been shown to strongly absorb calcium ions [43].

It has been demonstrated that nHA may be uptaken by cells and exhibit good intracellular release kinetics [44]. Size, shape, and surface charge are known to be key parameters that influence receptor-mediated cellular uptake [45]. Regardless of ZP, precipitated particles of samples 10-/RT/DI, 11-/RT/DI, 10+/RT/DI and 11+/RT/DI were shown to associate with cell membranes and be internalised without causing cytotoxic effects after 24hrs (Figure 8). This suggests that the source of toxicity, demonstrated for 10-/RT/DI using a dead/live assay (Figure 5), is an impurity phase not present in high quantities as implied from XRD and FTIR data.

5 Conclusions

The novelty of this work is attributed to the associations made between material properties and the biological performance of HA substrates prepared under different processing conditions. pH value and temperature were shown to be critical in precipitating a cytocompatible apatite phase. This is explained by the influence of these parameters on the concentration of different molecular species within solution throughout synthesis and this was shown to translate to the chemical composition of the precipitate, as evidenced by XRD, FTIR, DTA-TGA, and ZP measurements. A notable increase in proliferation of MC3T3 cells seeded on non-cytotoxic substrates produced under controlled pH conditions (10+/RT/DI and 11+/RT/DI) compared with uncontrolled (11-/RT/DI) was demonstrated using MTT and Hoechst assays, despite these samples exhibiting similar bulk compositions as analysed by XRD, FTIR and DTA-TGA. Suggesting that pH variations during synthesis may affect surface chemistry as well as bulk composition, and ultimately this translated to changes in cell behaviour *in-vitro*. Thus, these results advocate that it is vital to consider the absolute value of pH and that it is advantageous to maintain an initial reaction pH of 10 or 11 throughout synthesis in order to precipitate a substrate that is cytocompatible and supports a higher degree of cell proliferation.

The uses of Ethanolamine and/or Toluene in the solvent system for HA precipitation was not found to adversely affect cell viability. *In-vitro* results for HA prepared in systems containing Toluene (11+/RT/T) alone or with Ethanolamine (11+/RT/ET) are considered promising since the relative increase in the metabolic activity or number of MC3T3 osteoblast precursor cells seeded on substrates over the 7 day culture period was demonstrated. Notably, the crystallinity of these samples was relatively low and their surface area particularly high compared with a reference HA composition prepared under the same reaction conditions in DI water.

Overall, the results of this study advocate that pH should be maintained at 10 or 11 during precipitation to ensure that a non-cytotoxic precipitate is formed. Furthermore, this work highlights the potential application of alternative non-polar solvents to control and alter the physiochemical characteristics of HA that play an important role in determining the effectiveness of this material in bone tissue applications.

References

1. Kavitha, M., et al., *Optimization of process parameters for solution combustion synthesis of Strontium substituted Hydroxyapatite nanocrystals using Design of Experiments approach.* Powder Technology, 2015. **271**: p. 167-181.
2. Cox, S.C., R.I. Walton, and K.K. Mallick, *Comparison of Techniques for the Synthesis of Hydroxyapatite.* 2014.
3. Nayak, A.K., *Hydroxyapatite synthesis methodologies: an overview.* International Journal of ChemTech Research, 2010. **2**(2): p. 903-907.
4. Koutsopoulos, S., *Synthesis and characterization of hydroxyapatite crystals: a review study on the analytical methods.* Journal of Biomedical Materials Research, 2002. **62**(4): p. 600-612.
5. Cengiz, B., et al., *Synthesis and characterization of hydroxyapatite nanoparticles.* Colloids and Surfaces a-Physicochemical and Engineering Aspects, 2008. **322**(1-3): p. 29-33.
6. Drouet, C., *Apatite formation: why it may not work as planned, and how to conclusively identify apatite compounds.* BioMed research international, 2013. **2013**.
7. Liu, C., et al., *Kinetics of hydroxyapatite precipitation at pH 10 to 11.* Biomaterials, 2001. **22**(4): p. 301-306.
8. Bohner, M., *Calcium orthophosphates in medicine: from ceramics to calcium phosphate cements.* Injury-International Journal of the Care of the Injured, 2000. **31**: p. S37-S47.
9. Cunniffe, G.M., et al., *The synthesis and characterization of nanophase hydroxyapatite using a novel dispersant-aided precipitation method.* Journal of Biomedical Materials Research Part A, 2010. **95A**(4): p. 1142-1149.
10. Saeri, M.R., et al., *The wet precipitation process of hydroxyapatite.* Materials Letters, 2003. **57**(24-25): p. 4064-4069.
11. Afshar, A., et al., *Some important factors in the wet precipitation process of hydroxyapatite.* Materials & Design, 2003. **24**(3): p. 197-202.
12. Garcia, C., et al., *Effect of some physical-chemical variables in the synthesis of hydroxyapatite by the precipitation route.* Bioceramics, Vol 17, 2005. **284-286**: p. 47-50.
13. Rodriguez-Lorenzo, L.M. and M. Vallet-Regi, *Controlled crystallization of calcium phosphate apatites.* Chemistry of Materials, 2000. **12**(8): p. 2460-2465.
14. Kumta, P.N., et al., *Nanostructured calcium phosphates for biomedical applications: novel synthesis and characterization.* Acta Biomaterialia, 2005. **1**(1): p. 65-83.
15. Raynaud, S., et al., *Calcium phosphate apatites with variable Ca/P atomic ratio I. Synthesis, characterisation and thermal stability of powders.* Biomaterials, 2002. **23**(4): p. 1065-1072.
16. Wang, P.P., et al., *Effects of synthesis conditions on the morphology of hydroxyapatite nanoparticles produced by wet chemical process.* Powder Technology, 2010. **203**(2): p. 315-321.
17. Pang, Y.X. and X. Bao, *Influence of temperature, ripening time and calcination on the morphology and crystallinity of hydroxyapatite nanoparticles.* Journal of the European Ceramic Society, 2003. **23**(10): p. 1697-1704.
18. Bouyer, E., F. Gitzhofer, and M.I. Boulos, *Morphological study of hydroxyapatite nanocrystal suspension.* Journal of Materials Science-Materials in Medicine, 2000. **11**(8): p. 523-531.
19. Vandecandelaere, N., C. Rey, and C. Drouet, *Biomimetic apatite-based biomaterials: on the critical impact of synthesis and post-synthesis parameters.* Journal of Materials Science: Materials in Medicine, 2012. **23**(11): p. 2593-2606.

20. Jarcho, M., et al., *Hydroxylapatite synthesis and characterization in dense polycrystalline form.* Journal of Materials Science, 1976. **11**(11): p. 2027-2035.
21. Xue, W., et al., *Osteoprecursor cell response to strontium-containing hydroxyapatite ceramics.* Journal of Biomedical Materials Research Part A, 2006. **79**(4): p. 804-814.
22. Smith, A.M., et al., *Nanoscale crystallinity modulates cell proliferation on plasma sprayed surfaces.* Materials Science and Engineering: C, 2015. **48**: p. 5-10.
23. Cox, S.C., et al., *Low temperature aqueous precipitation of needle-like nanophase hydroxyapatite.* Journal of Materials Science: Materials in Medicine, 2014. **25**(1): p. 37-46.
24. Williams, R.L., et al., *Thiol modification of silicon-substituted hydroxyapatite nanocrystals facilitates fluorescent labelling and visualisation of cellular internalisation.* J. Mater. Chem. B, 2013.
25. Rodriguez-Lorenzo, L. and M. Vallet-Regi, *Controlled crystallization of calcium phosphate apatites.* Chemistry of Materials, 2000. **12**(8): p. 2460-2465.
26. Dorozhkin, S.V. and M. Epple, *Biological and medical significance of calcium phosphates.* Angewandte Chemie-International Edition, 2002. **41**(17): p. 3130-3146.
27. Yuasa, T., et al., *Effects of apatite cements on proliferation and differentiation of human osteoblasts in vitro.* Biomaterials, 2004. **25**(7): p. 1159-1166.
28. McIntosh, A. and W. Jablonski, *X-ray diffraction powder patterns of calcium phosphates.* Analytical Chemistry, 1956. **28**(9): p. 1424-1427.
29. Mortier, A., J. Lemaitre, and P.G. Rouxhet, *Temperature-programmed characterization of synthetic calcium-deficient phosphate apatites.* Thermochimica Acta, 1989. **143**(0): p. 265-282.
30. Elliott, J.C., *Structure and chemistry of the apatites and other calcium orthophosphates*. Vol. 4. 1994: Elsevier Amsterdam.
31. Eanes, E., I. Gillessen, and A. Posner, *Intermediate states in the precipitation of hydroxyapatite.* Nature, 1965. **208**: p. 365-367.
32. Newesely, H., *Changes in crystal types of low solubility calcium phosphates in the presence of accompanying ions.* Archives of Oral Biology, 1961. **6**: p. 174-180.
33. Betts, F. and A. Posner, *An X-ray radial distribution study of amorphous calcium phosphate.* Materials Research Bulletin, 1974. **9**(3): p. 353-360.
34. De Rooij, J., J. Heughebaert, and G. Nancollas, *A pH study of calcium phosphate seeded precipitation.* Journal of Colloid and Interface Science, 1984. **100**(2): p. 350-358.
35. Botelho, C., et al., *Structural analysis of Si-substituted hydroxyapatite: zeta potential and X-ray photoelectron spectroscopy.* Journal of Materials Science: Materials in Medicine, 2002. **13**(12): p. 1123-1127.
36. Morgan, J., et al., *In vitro mineralization and implant calcium phosphate-hydroxyapatite crystallinity.* Implant Dentistry, 1996. **5**(4): p. 264-271.
37. de Bruijin, J., et al., *Analysis of the bony interface with various types of hydroxyapatite in vitro.* Cells and Materials(USA), 1993. **3**(2): p. 115-127.
38. Termine, J.D., et al., *Osteonectin, a bone-specific protein linking mineral to collagen.* Cell, 1981. **26**(1): p. 99-105.
39. Sodek, J., B. Ganss, and M. McKee, *Osteopontin.* Critical Reviews in Oral Biology & Medicine, 2000. **11**(3): p. 279-303.
40. Maxian, S.H., et al., *Bone cell behavior on Matrigel®-coated Ca/P coatings of varying crystallinities.* Journal of Biomedical Materials Research, 1998. **40**(2): p. 171-179.
41. Davies, J.E., *In vitro modeling of the bone/implant interface.* The Anatomical Record, 1996. **245**(2): p. 426-445.

42. Albrektsson, T. and C. Johansson, *Osteoinduction, osteoconduction and osseointegration.* European Spine Journal, 2001. **10**: p. S96-S101.
43. Gustavsson, J., et al., *Ion reactivity of calcium-deficient hydroxyapatite in standard cell culture media.* Acta biomaterialia, 2011. **7**(12): p. 4242-4252.
44. Sokolova, V., et al., *Calcium phosphate nanoparticles as versatile carrier for small and large molecules across cell membranes.* Journal of Nanoparticle Research, 2012. **14**(6): p. 1-10.
45. Chen, L., et al., *The role of surface charge on the uptake and biocompatibility of hydroxyapatite nanoparticles with osteoblast cells.* Nanotechnology, 2011. **22**(10): p. 105708.

Figure and Table Captions

Figure 1: XRD data highlighting the variation in crystallinity of as-synthesised apatite samples prepared under different processing conditions (bottom to top); 10-/RT/DI (black); 11+/70/DI (blue); 11+/RT/DI (red); 11+/RT/T (green); 11+/RT/ET (purple); ♦ HA (09-0432).

Figure 2: Effect of heating apatite samples prepared under different pH conditions on the bulk composition as analysed by XRD (bottom to top); 10-/RT/DI (black); 10+/RT/DI (blue); 11-/RT/DI (red); 11+/RT/DI (green); ♦ HA (09-0432); ● β-TCP (09-0169); ▲ β-$Ca_2P_2O_7$ (09-0346).

Figure 3: FTIR spectra of selected apatite samples (bottom to top); 10-/RT/DI (black); 10+/RT/DI (blue); 11-/RT/DI (red); 11+/RT/DI (green); 11+/RT/T (purple). Data collected 1750 – 4000cm^{-1} and 550 – 1750cm^{-1} plotted on y_{left} and y_{right} axes, respectively.

Figure 4: Thermal behaviour of a) 10-/RT/DI; b) 10+/RT/DI; c) 11+/RT/DI; d) 11+/70/DI between 30 - 1300°C.

Figure 5: Cytotoxic effect of apatite samples a) 10-/RT/DI (day 1); b) 11+/RT/DI (day 1); and 11+/RT/DI (day 3) on cultured MC3T3 osteoblast precursor cells analysed via a live (green) dead (red) assay.

Figure 6: Fluorescence micrographs of sample 11+/RT/DI highlighting cytocompatibility and an increase in MC3T3 cell density over the culture period a) day 1; b) day 3; c) day 5; and d) day 7 (scale bar = 100μm).

Figure 7: The MTT results of MC3T3 cells grown on different HA substrates and tissue culture plastic (TP) as a positive control. Results presented are mean of n=9 specimens ± standard deviation.

Figure 8: Cellular internalisation of precipitated HA particles a) 10-/RT/DI, b) 11-/RT/DI, c) 10+/RT/DI, and d) 11+/RT/DI

Table 1: Summary of synthesis conditions used during the aqueous precipitation of reported hydroxyapatite samples. Sample coding refers to pH level and control/synthesis temperature/Ca solute concentration/Solvent system.

Table 2: Influence of precipitation synthesis conditions on the crystallite size, zeta potential and surface area analysis of apatite samples

Table 3: Influence of synthesis conditions on the proliferative rate of MC3T3 osteoblast precursor cells. *Statistical significance calculated using one-way ANOVA test and set at $p<0.05$.

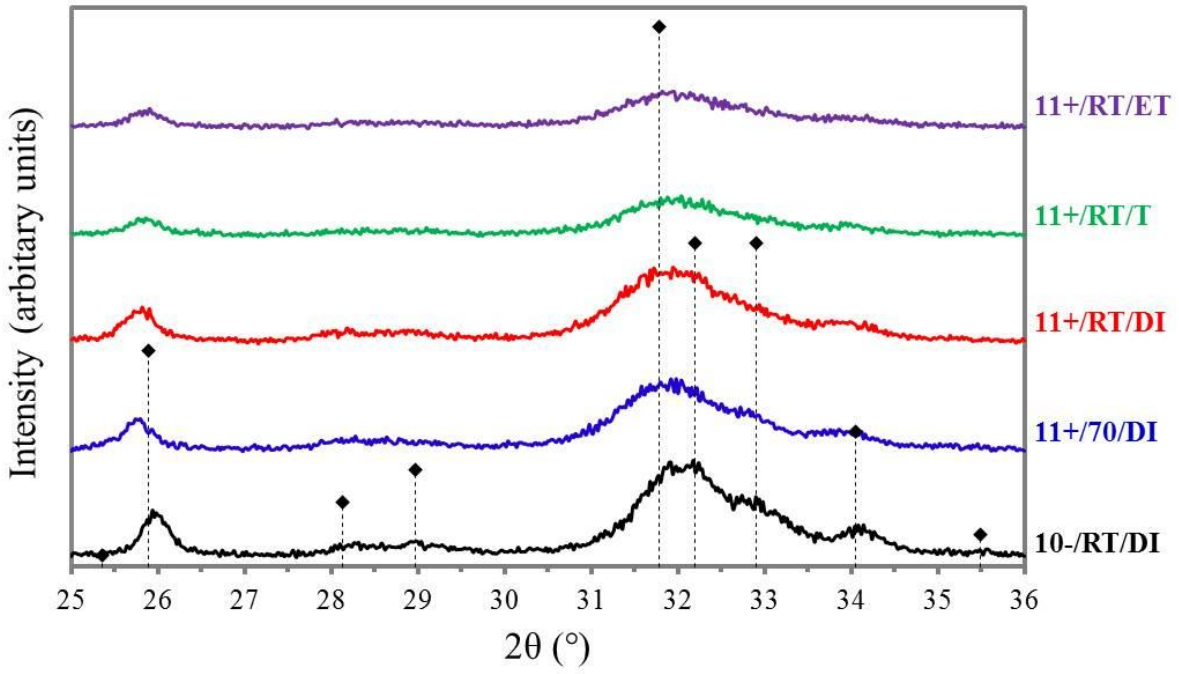

Figure 1

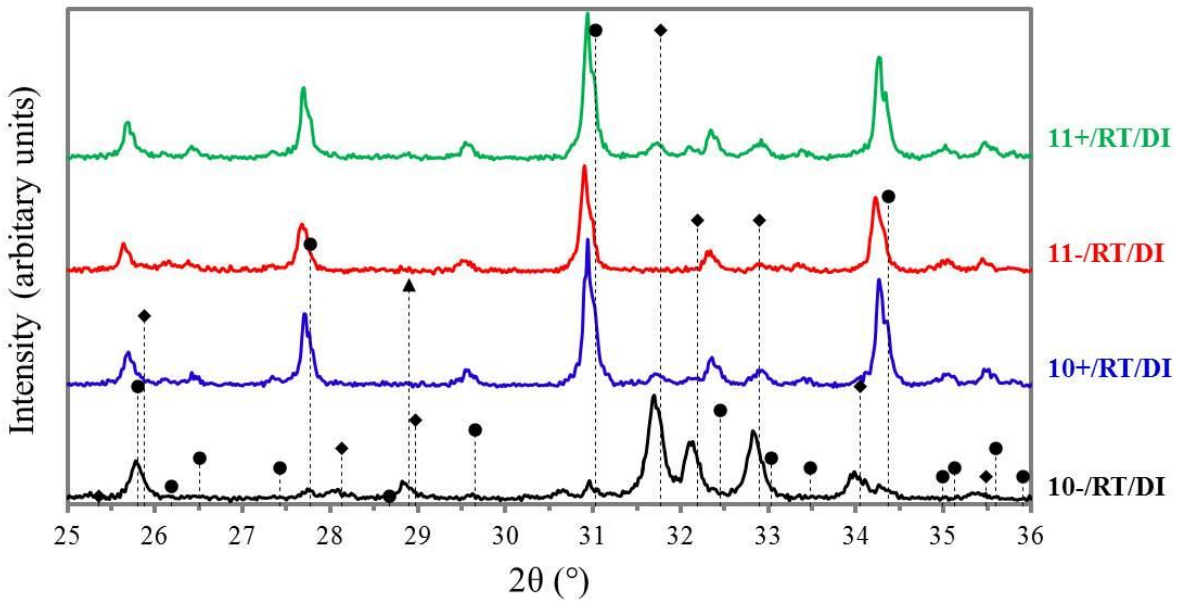

Figure 2

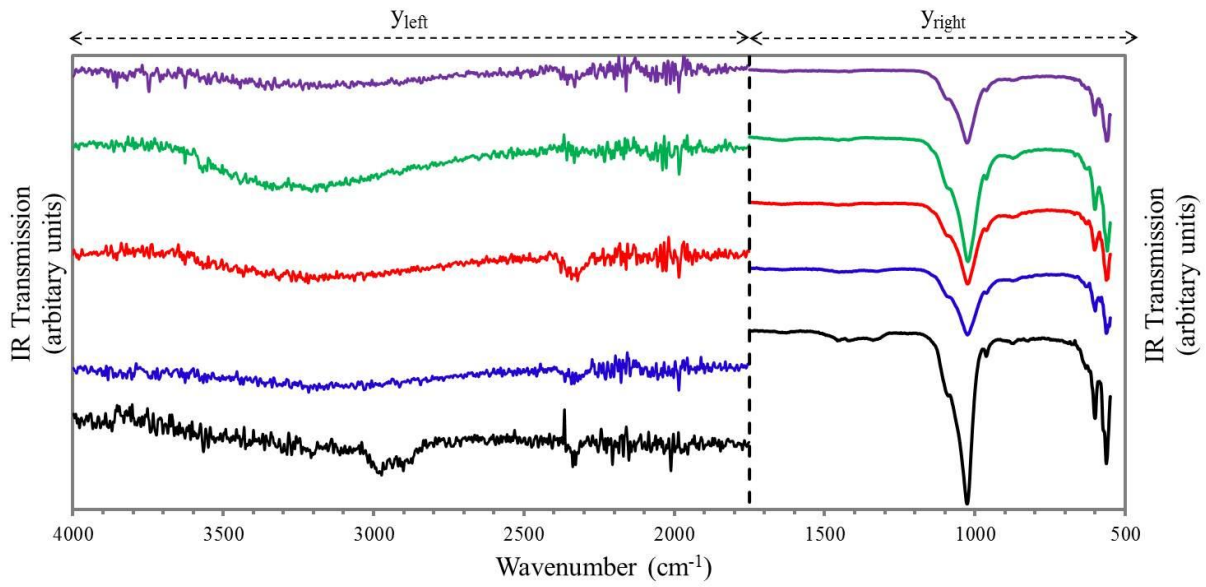

Figure 3

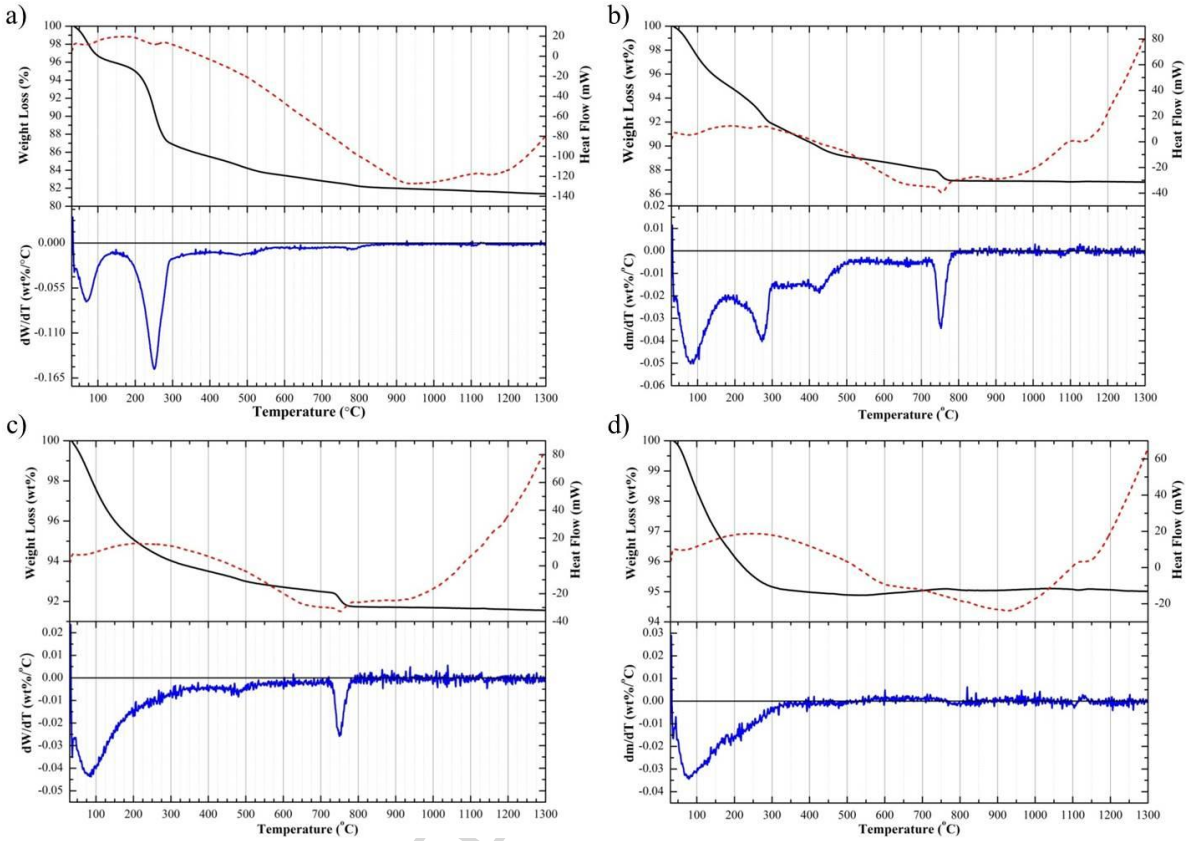

Figure 4

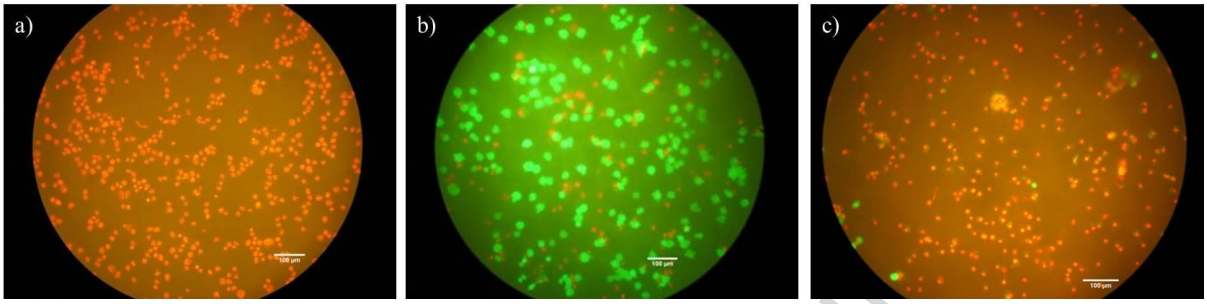

Figure 5

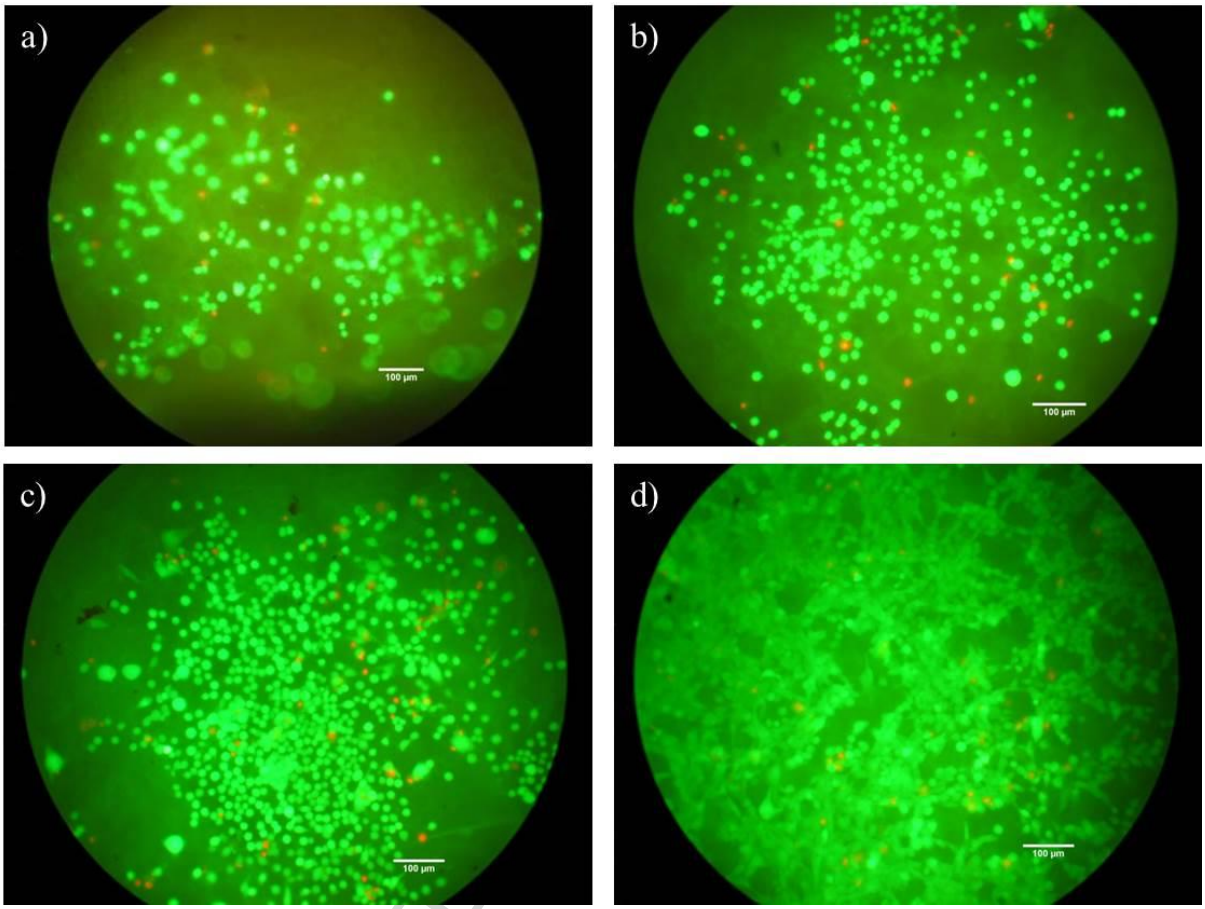

Figure 6

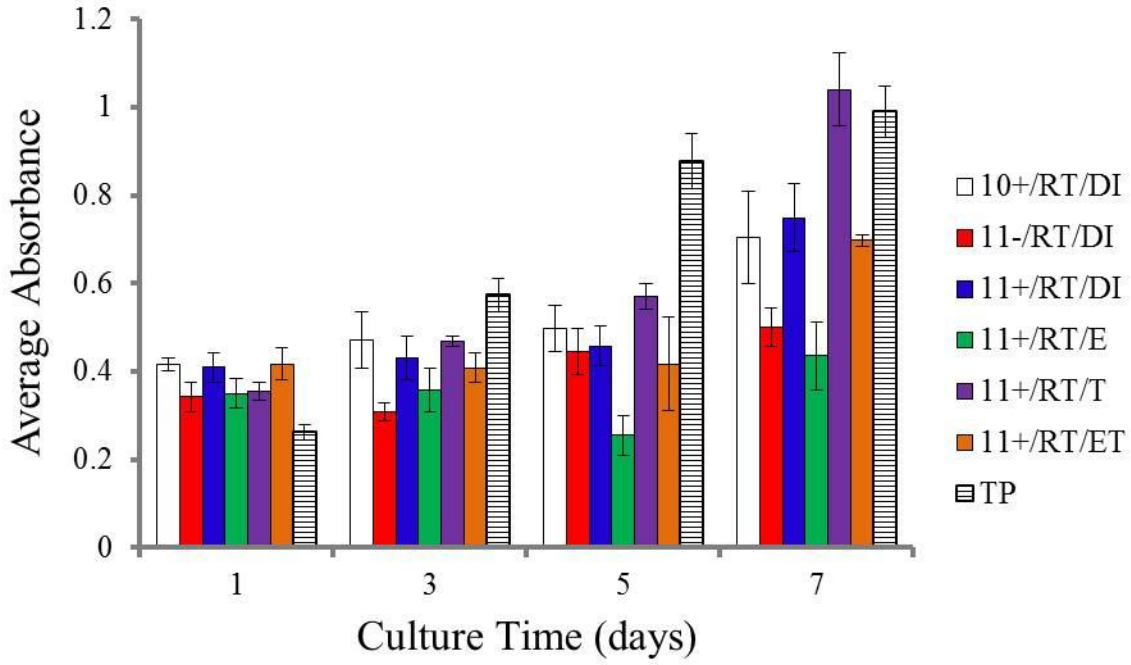

Figure 7

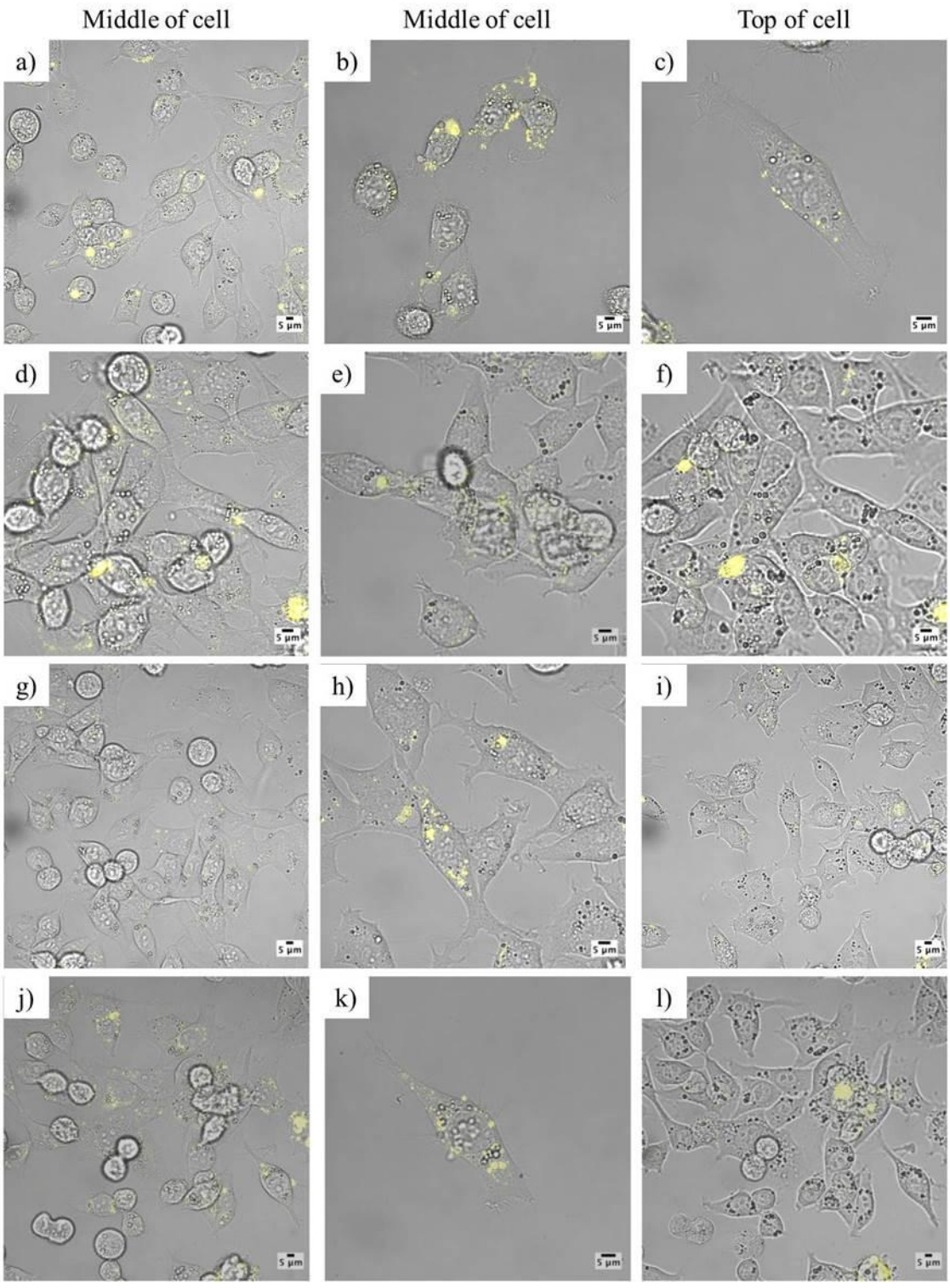

Figure 8

Sample code	pH level	pH control	Synthesis temperature (°C)	Solvent System
10-/RT/DI	10	Uncontrolled	20	DI water
11-/RT/DI	11	Uncontrolled	20	DI water
10+/RT/DI	10	Controlled	20	DI water
11+/RT/DI	11	Controlled	20	DI water
11+/70/DI	11	Controlled	70	DI water
11+/RT/E	11	Controlled	20	DI water, 5wt% Ethanolamine
11+/RT/T	11	Controlled	20	40% DI water, 60% Toluene
11+/RT/ET	11	Controlled	20	40% DI water, 60% Toluene, 5wt% Ethanolamine*

Table 1: Summary of synthesis conditions used during the aqueous precipitation of reported hydroxyapatite samples. Sample coding refers to pH level and control/synthesis temperature/Ca solute concentration/Solvent system. *Added to the initial DI water and Toleue solvent system after the addition of calcium nitrate.

Sample code	Crystallite Size (nm)	Zeta Potential (mV)	Surface Area (m^2/g)
10-/RT/DI	24	0.525	72.7±0.1
11-/RT/DI	21	-16.8	100±0.2
10+/RT/DI	22	-19.1	104.1±0.2
11+/RT/DI	20	-21.3	106.7±0.2
11+/70/DI	21	2.98	132.3±0.7
11+/RT/E	20	-5.22	106.2±0.4
11+/RT/T	22	-5.21	126.1±0.6
11+/RT/ET	22	-2.85	110.2±0.5

Table 2: Influence of precipitation synthesis conditions on the crystallite size, zeta potential and surface area analysis of apatite samples

Sample	MTT assay		Hoechst assay	
	Proliferative rate (%)	Day 7 *F* ratio	Proliferative rate (%)	Day 7 *F* ratio
11-/RT/DI	46.3	50.215*	42.3	2.887
10+/RT/DI	68.7	44.015*	626.0	507.364*
11+/RT/DI	82.8	96.317*	495.7	106.892*
11+/RT/E	24.6	29.069*	431.0	137.446*
11+/RT/T	193.5	388.765*	467.7	16.937*
11+/RT/ET	67.4	297.140*	538.9	162.713*

Table 3: Influence of synthesis conditions on the proliferative rate of MC3T3 osteoblast precursor cells. *Statistical significance calculated using one-way ANOVA test and set at $p<0.05$.

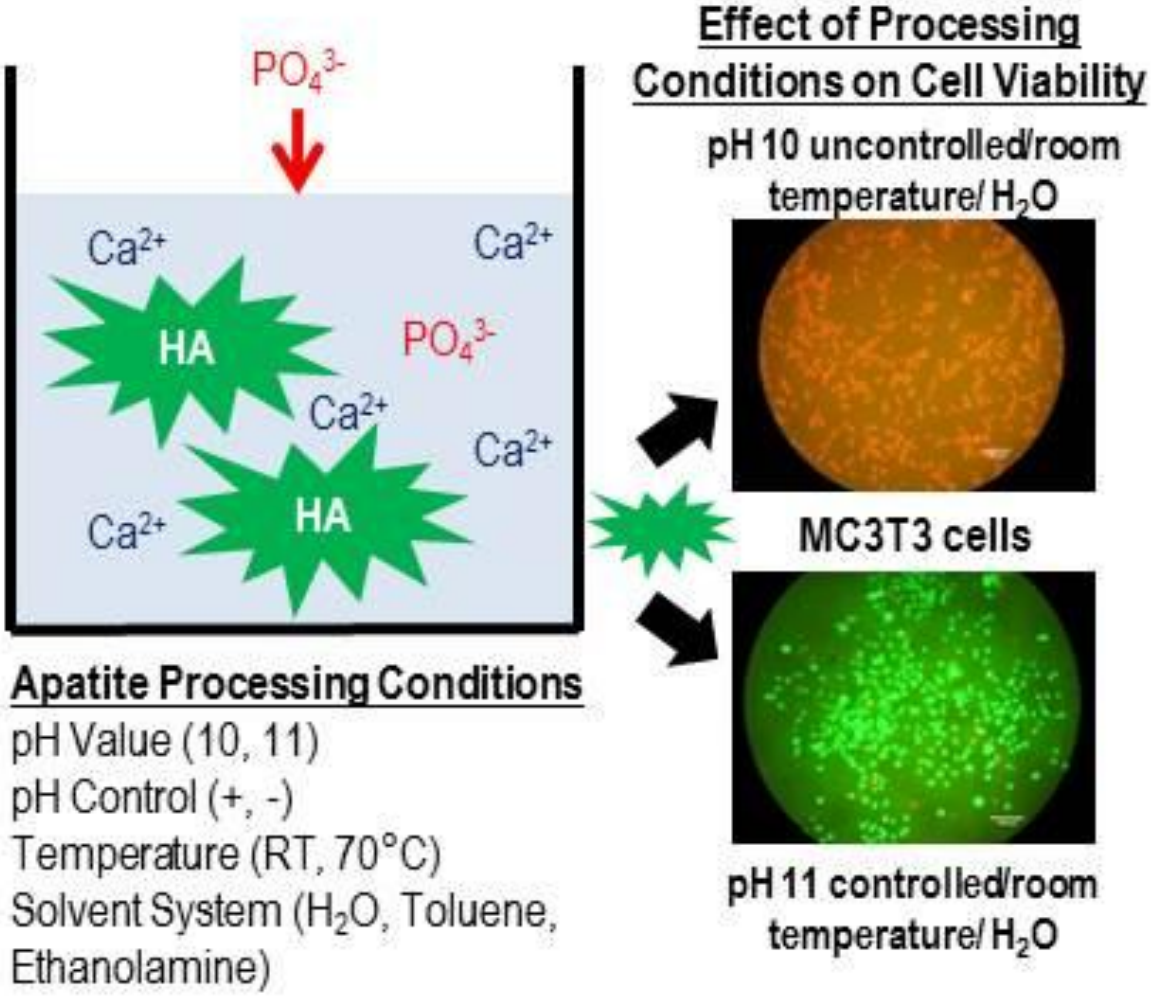

Graphical abstract

The importance of processing conditions on the biological response to apatites

Highlights

- Hydroxyapatite cytocompatibility may be compromised by processing conditions
- pH value and control during apatite synthesis affects bulk and surface chemistry
- Cell proliferation was improved by maintaining pH at 10 or 11 during HA synthesis
- Non-polar solvents may be advantageously used to alter precipitate properties
- Toluene significantly reduced crystallinity and increased precipitate surface area